CHEMICAL ENGINEERING TRANSACTIONS
VOL. 86, 2021
A publication of AIDIC
The Italian Association of Chemical Engineering
Online at www.cetjournal.it
Guest Editors: Sauro Pierucci, Jiří Jaromír Klemeš

ISBN 978–88–95608–84–6; **ISSN** 2283–9216

Influence of the liquid viscosity on the properties of gas bubbles formed in co–current flow

Mateusz Prończuk, Przemysław Luty, Katarzyna Bizon*

Faculty of Chemical Engineering and Technology, Cracow University of Technology, ul. Warszawska 24, 31–155 Kraków, Poland
katarzyna.bizon@pk.edu.pl

A wide range of physical and chemical processes of considerable industrial relevance rely on bubble flows. These include wastewater treatment, mineral and oil processing, fermentation or food treatment. A proper design of such processes requires the determination of hydrodynamic properties of single bubbles and of bubble swarms. This, in turn, involves the need for the development of reliable models, that are usually made of empirically derived correlations. There is a great number of experimental works dealing with determination of the hydrodynamic properties of gas bubbles rising in a stagnant liquid, but not many cover the case of co-current flow of dispersed gas and liquid. The aim of this study is to determine an empirical correlation to predict the drag coefficient of a single bubble during its formation in co-currently flowing liquid, as well as its equivalent diameter. A shadowgraphy technique is employed to determine experimentally the diameters of single gas bubbles formed in flowing in co-current liquid. The influence of the liquid viscosity on the forming bubble is evaluated. Based on the balance of forces affecting the bubble, the obtained experimental results are then used to determine correlations that permit to predict the drag coefficient and the bubble diameter. The derived models vary significantly from those available in the literature, but they show a much better agreement with the experimental data.

1. Introduction

Two-phase gas-liquid flow is widely described in a scientific literature. According to Google Scholar, searching for phrase "gas liquid flow" leads to 1.3 million scientific articles published in the last decade (2011–2020). The two-phase gas-liquid flows have also found many applications in various fields of industry. Processes in which the phenomenon of bubbling occurs are of particular interest. Apart from bubble columns and their modifications (e.g. airlift apparatus), the phenomenon of bubbling can be encountered in absorption and rectification towers, tank apparatuses, and various types of chemical reactors (Merchuk, 2003). Bubbling is employed in various fields of industry, as among others to conduct microbiological processes, in wastewater treatment processes, crude oil processing and even in metallurgy (Kulkarni and Joshi, 2005).

The properties of gas bubbles formed in non-flowing liquid have so far been relatively comprehensively studied and well understood. Numerous reports on the formation of gas bubbles were published in the literature for decades, some of them more than a century ago (Hadamard, 1911). There are many publications describing determination of a diameter, slip velocity, drag coefficient and other properties of gas bubbles formed in both Newtonian and non-Newtonian fluids. However, there is a significant shortage of studies describing the properties of bubbles formed in the flowing liquid. In industry, one most often deals with the flow of bubbles in a co-current mode. Such a situation occurs in airlift apparatuses and, in some cases, in bubble columns (Kulkarni and Joshi, 2005).

In the literature, one can find only a few papers describing the formation of bubbles in a fluid flowing in co-current (Chuang and Goldschmidt, 1970; Sada et al., 1978; Terasaka et al., 1999; Muilwijk and Van den Akker, 2019). The authors agree that the co-current flow of the liquid does not affect the slip velocity of gas bubbles. The flow of the liquid only affects the diameter of the bubbles formed, causing the size of the bubbles formed to decrease as the velocity of the liquid flow increases. This is due to the presence of additional force during bubble formation – the drag force arising from the friction of the flowing liquid against the gas bubble

surface. Each of the work dealing with this problem presents a slightly different approach to the description of bubble formation in a co-currently flowing fluid. Nevertheless, the correlations available in the literature can be divided basically into two main groups: models based on the force balance and experimental models based on dimensionless numbers. One of the models based on the dimensionless numbers was proposed by Sada et al. (1978). In their work, the authors used the modified Froude number defined as:

$$\mathrm{Fr}_{mod} = \frac{u_G^2}{g d_b + 0.33 u_{0L}^2} \tag{1}$$

where u_G – gas velocity, m/s; g – gravitational acceleration, m/s^2; d_b – bubble diameter, m; u_{0L} – superficial liquid velocity, m/s. The bubble diameter can be calculated as:

$$\frac{d_b}{d_i} = a\mathrm{Fr}_{mod}^{b} \tag{2}$$

where d_i – orifice internal diameter, m; a, b – equation constants, dimensionless. Muilwijk and Van den Akker (2019) proposed an alternative correlation based on dimensionless Bond, Bo, and Froude, Fr numbers in their classical definition. In their model the influence of the liquid velocity was taken into account by applying the ratio of the liquid and gas velocity, denoted respectively with u_L and u_G:

$$\frac{d_b}{d_i} = \left((9.01\mathrm{Bo}^{-0.80} + 1.57\mathrm{Fr}^{0.58})^{-1} + 0.06\left(\frac{u_L}{u_G}\right)^{0.80} \right)^{-1/3} \tag{3}$$

Another approach to determine the bubble diameter is based on the force balance. The model proposed by Chuang and Goldschmidt (1970) accounts for the forces of buoyancy, drag, surface tension and added mass inertial force:

$$\frac{\pi d_b^3 \rho_L g}{6} + c_D A_D \left(u_L - \frac{ds}{dt}\right)^2 \frac{\rho_L}{2} = \pi d_i \sigma_L + \frac{1}{2}\frac{d}{dt}\left(M\frac{ds}{dt}\right) \tag{4}$$

where ρ_L – liquid density, kg/m^3; c_D – drag coefficient, dimensionless; A_D – area of influence of drag force, m^2; u_L – liquid velocity, m/s; s – displacement of the center of mass of the bubble, m; t – time, s; σ_L – liquid surface tension, N/m; M – mass, kg. Terasaka et al. (1999) used a similar approach as in Eq. (5), but they additionally considered the gas phase momentum flux:

$$\frac{\pi d_b^3 (\rho_L - \rho_G) g}{6} + c_D A_D \left(u_L - \frac{ds}{dt}\right)^2 \frac{\rho_L}{2} + \frac{4\rho_G Q_{VG}^2}{\pi d_i^2} = \pi d_o \sigma_L + \frac{1}{2}\frac{d}{dt}\left(M\frac{ds}{dt}\right) \tag{5}$$

where ρ_G – gas phase density, kg/m^3; Q_{VG} is gas volumetric flow rate, m^3/s; d_o – orifice outer diameter, m.

To describe the influence of the drag force, the authors usually use correlations intended for the gas bubbles rising in a stagnant liquid layer (Chuang and Goldschmidt, 1970; Terasaka et al., 1999). This approach can lead to erroneous results, since in the case of bubble formation in the flowing liquid, the velocity of the liquid can vary independently of the bubble diameter, while in the case of bubble rising in the stagnant liquid, the rise velocity and diameter are closely related. Thus, the aim of this study was to determine the values of the drag coefficients depending on the physical properties of the liquid phase.

2. Materials and methods

2.1 Experimental stand

The scheme of the research stand is presented in Figure 1. The liquid was stored and pumped from the tank (denoted with number 1 in Fig. 1). The liquid flow rate was provided by the liquid centrifugal pump (2 in Fig. 1) and was controlled by two liquid valves, i.e., the main liquid valve (4 in Fig. 1) and the bypass valve (3 in Fig. 1). This was to prevent excessive throttling of the pump at low overall flow rates. The liquid flow rate was measured using an ultrasonic flowmeter (5 in Fig. 1). The main element of the experimental setup was a bubbling zone located in a column of a square section with an inner side length of 0.08 m made of poly(methyl methacrylate) (6 in Fig. 1). The liquid was introduced at the bottom of the column (7 in Fig. 1) and before reaching the bubbling zone it was flowing through two layers of packing consisting of Raschig rings of diameters equal to 5 mm and 16 mm, respectively (8 in Fig. 1), so as to flatten the liquid velocity profile. Then, the liquid was flowing through the two layers of flow straighteners made of pipes of low diameter in order to laminarize the liquid flow (9 in Fig. 1). One additional layer of flow straighteners was located above the bubbling zone to reduce the stream contraction effect in the upper part of the column. The air introduction to the bubble zone of the column was provided by an air compressor (10 in Fig. 1). The air flow rate was controlled with the use of an air valve (11 in Fig. 1). It was introduced through a brass orifice with internal and external diameters equal, respectively, to 0.8 mm and to 1.0 mm (12 in Fig. 1). The orifice length was about 0.15 m, wherein the length of its straight outlet section was equal to 15 mm to provide a laminar gas flow profile at the tip of the orifice. The orifice was bent at an angle of 90°. It was partially immersed in the liquid and its straight outlet part was located about 0.1 m above the top of the second flow straightener. The outlet

part of the orifice was oriented vertically upwards. The two-phase exhaust mixture of the liquid and the gas was leaving the column through an outlet placed in the upper part of the column (13 in Fig. 1). The liquid temperature was measured at the column outlet using a thermometer (14 in Fig. 1). After leaving the column, the mixture was flowing to the tank, where the excess air was being evacuated. There was, however, a full recirculation of the liquid phase. The films showing the formation and the flow of gas bubbles were recorded using a CMOS IDS UI-3130CP-C-HQ Rev.2 camera that enables high-frequency image recording (15 in Fig. 1). It allows to record videos with a frequency equal to about 550 fps. LED lightning was placed on the back side of the bubble column (16 in Fig. 1).

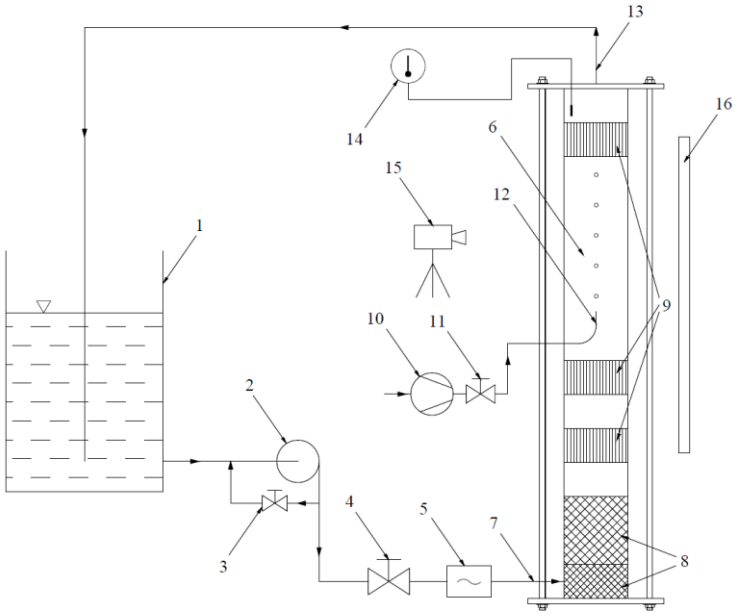

Figure 1: Scheme of the research stand: 1 – liquid tank, 2 – liquid pump, 3 – liquid bypass valve, 4 – main liquid valve, 5 – ultrasonic flowmeter, 6 – bubbling zone, 7 – liquid inlet, 8 – Raschig rings, 9 – flow straighteners, 10 – air compressor, 11 – air valve, 12 – orifice, 13 – liquid and gas outlet, 14 – thermometer, 15 – high-speed camera connected to PC, 16 – LED backlight.

2.2 Materials

In this study, aqueous solution of technical-grade glycerol and tap water were used as liquid phases and air was used as the gas phase. Water/glycerol solution (50 wt% glycerol) temperature varied from 20°C to 26°C due to pump self-heating. Tap water was supplied from the water mains and its temperature was constant and equal to 12°C. Air was injected to the liquid through an orifice. The air inlet temperature was about 20°C and did not significantly change while injecting to the liquid, nor while flowing upwards after the bubble detachment from the orifice due to a small temperature difference between the liquid and the air. Furthermore, since there is no significant influence of the temperature on air density in the considered temperature range, it was assumed to be constant. The physical properties of the liquid phases and the gas phase utilized in calculations are shown in Table 1.

Table 1: Physical parameters of the liquid phases and the gas phase utilized in calculations

Parameter	Symbol	Value/formula		Unit
		Water/glycerol	Water	
Liquid density	ρ_L	–0.693T+1.160	999.7	kg/m^3
Liquid kinematic viscosity	ν_L	–0.256T+12.1	1.31	mm^2/s
Liquid surface tension	σ_L	–0.131T+60.4	74.2	mN/m
Gas density	ρ_G	1.20	1.20	kg/m^3

2.3 Experimental procedures

The method for determination of a bubble diameter was a non-invasive shadowgraphy method (Nishino et al., 2010). The light emitted by a LED lamp refracted on the gas-liquid interfacial surface. This phenomenon was

visible in the recorded images as a dark rim around the bubble. To extract geometrical properties of the bubbles from recorded video an image analysis based on in-built Matlab functions was performed. The processing of each frame involved three main stages. Firstly, a colour image showing a gas bubble was converted to a grayscale image. Secondly, the resulting grayscale image was compared with a frame with no bubbles (i.e., background image), previously also converted to a grayscale. Finally, the resulting image was converted to a binary one by utilization of an appropriate threshold. The stages of image processing are shown in Figure 2.

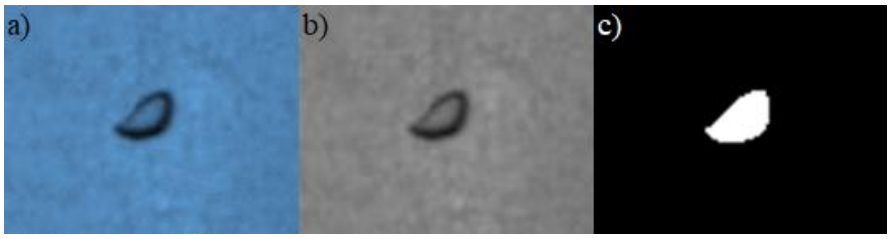

Figure 2: Selected stages of image processing; a) colour image, b) grayscale image, c) binary image

Basing on the final binary image, the projection surface of the bubble, expressed in pixels, was determined with the use of Matlab *regionprops* function. The next step was the calculation of a projection diameter, i.e. a diameter of a circle with a surface equal to a bubble projection surface. In order to express the bubble projection diameter in a unit of length, its value in pixels was multiplied by an appropriate constant resulting from a distance between the bubble column and the camera. The above procedure may be represented by the following formula (6):

$$d_b = \left(\frac{4S}{\pi}\right)^{0.5} \cdot C_{mp} \tag{6}$$

where S – bubble projection surface, pixels; C_{mp} – conversion factor for conversion diameter in pixels to meters, m/pixel.

The frequency of the bubble formation was below one bubble per second. For such a low frequency the influence of the drag force due to the wake of the previous bubble on the newly formed bubble is negligible. Hence, the formation of each bubble was very close to a static formation.

2.4 Mathematical model

A mathematical model of bubble formation proposed in a previous study by Luty and Prończuk (2020) was implemented. It is based on a balance of forces acting on the bubble during its formation. The key parameter of the model is bubble drag coefficient, c_D. The force balance equation can be written as:

$$\frac{\pi d_b^3 \rho_L g}{6} + c_D A_D \left(u_L - \frac{d_b f}{6}\right)^2 \frac{\rho_L}{2} = \pi d_i \sigma_L \tag{7}$$

where f – frequency of bubble formation, 1/s.

After transformations, the above equation can be presented in a form that allows calculation of the bubble drag coefficient, namely:

$$c_D = \frac{6\pi d_i \sigma_L - \pi d_b^3 \rho_L g}{3A_D \left(u_L - \frac{d_b f}{6}\right)^2 \rho_L} \tag{8}$$

In the work of Luty and Prończuk (2020) it was proved, that the surface of the bubble affected by the drag force should be expressed as bubble projection surface, i.e.:

$$A_D = \frac{\pi d_b^2}{4} \tag{9}$$

Combining Eq. (8) with Eq. (9) yields:

$$c_D = \frac{24 d_i \sigma_L - 4 d_b^3 \rho_L g}{3 d_b^2 \left(u_L - \frac{d_b f}{6}\right)^2 \rho_L} \tag{10}$$

To determine Reynolds number, it is necessary to select an appropriate characteristic velocity. The relative velocity between the central point of the bubble and the flowing liquid was used for this purpose. The liquid velocity considered is a local liquid velocity in the axis of the column and not its average velocity in the apparatus. Luty and Prończuk (2020) demonstrated that the characteristic length used in Reynolds number should be a difference between bubble diameter, d_b, and orifice internal diameter, d_i. Therefore, the Reynolds number definition is as follows:

$$\mathrm{Re} = \frac{\left(u_L - \frac{d_b f}{6}\right)\rho_L (d_b - d_i)}{\mu_L} \tag{11}$$

where μ_L – liquid dynamic viscosity, Pa·s. To determine the liquid local velocity in the axis of the column as a function of the average liquid flow rate, the series of tracer experiments was performed. Small amounts of tracer, a diluted solution of blue ink in the aqueous solution of glycerol, were injected through the orifice instead of air. The tracer settling velocity was determined in the same way as for described above. The calculated settling velocity of the tracer, u_t, turned out to be equal to:

$$u_t = 2.0 \cdot 10^{-3}\ \mathrm{m/s} \tag{12}$$

where u_t – tracer settling velocity, m/s. The above value was added to the experimentally obtained local tracer flow velocity in the axis of the column giving, in consequence, a local liquid velocity.

3. Results

3.1 Liquid velocity

The liquid flow velocity in the axis of the bubble zone of the column, u_L, was determined for various values of the liquid flow rate, Q_{VL}, in the range of 240–1505 dm^3/h in the case of the water-glycerol mixture. The experimentally obtained values were then approximated using the following quadratic equation:

$$u_L = 1.26 \cdot 10^{-8} Q_{VL}^2 + 1.25 \cdot 10^{-5} Q_{VL} + 2.86 \cdot 10^{-2} \tag{13}$$

For the case of water as the liquid phase, the velocity equations presented in the work of Luty and Prończuk (2020) were used.

3.2 Drag coefficient values and correlation

The drag coefficient values were correlated with the values of the Reynolds number for the case of bubble formation in the flowing liquid. Eq. (10) was applied as a definition of the drag coefficient and Eq. (11) as a definition of the Reynolds number. In order to correlate the above parameters, a power model was used for regression according to the following equation:

$$c_D = a\mathrm{Re}^b \tag{14}$$

The power model is frequently used to correlate the drag coefficient depending on the Reynolds number (Kulkarni and Joshi, 2005). There is a necessity to determine values of constants a and b in the above equation. The formula for the water-glycerol solution used in this work has the following form:

$$c_D = 164\mathrm{Re}^{-1.29} \tag{15}$$

For the tap water the equation becomes:

$$c_D = 64400\mathrm{Re}^{-1.98} \tag{16}$$

The values of parameters a and b in Eq. (15) differ from the values of these parameters obtained for tap water (Eq. (16)) reported also in the work of Luty and Prończuk (2020). The comparison of experimental data and approximating equations for bubble formation in both tap water and aqueous solution of glycerol are shown in Figure 3a. All results shown in the Figure 3a concern the orifice internal and external diameter of 0.0008 m and 0.001 m respectively.

3.3 Validation of the correlation

In order to verify the correctness of the obtained correlations, their validation was carried out. Based on the obtained correlations, gas bubbles diameter was determined using the Eq. (7). Eq. (15) was used to calculate the diameters for the water/glycerol–air system, and the Eq. (16) for the water–air system. The obtained results are very consistent with the experimental data. Most of the calculated diameters do not differ from the experimental ones by more than ±5%. Obtained results are shown in Figure 3b.

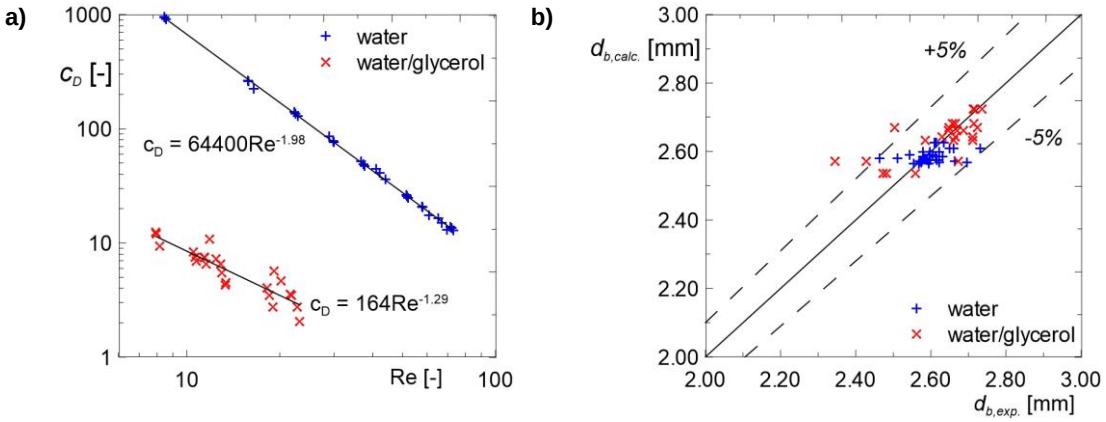

Figure 3: a) drag coefficient, c_D, versus Reynolds number, Re; b) experimental values of the bubble diameter, $d_{b,exp.}$, versus calculated bubble diameter, $d_{b,calc}$.

4. Discussion and conclusions

To describe the bubble formation phenomenon in a flowing liquid, correlations for the drag coefficient for bubble rise in a non-flowing liquid are usually used. The research carried out in this study allowed to obtain mathematical correlations for determination of the drag coefficient in flowing liquid. These correlations are significantly different from those available in the literature for bubble rise in non-flowing liquid. This may be caused by the connection of the bubble with the orifice before its detachment. As a result, the velocity of the liquid flowing around the bubble can be freely varied, as opposed to the rising in a non-flowing liquid, where the rise velocity (and hence the drag coefficient) is a function of only the bubble diameter and physical properties of gas and liquid.

The study also investigated the influence of physical properties of the liquid phase. Tap water and an aqueous solution of technical-grade glycerol were used as the liquid phases. The viscosity of this solution was about 700% higher than that of tap water. On the other hand, the density was about 15% higher and the surface tension was about 23% lower than for the tap water. As can be seen in Figure 3a, the coefficients of the exponential equation describing the dependence of the drag coefficient on the Reynolds number have a completely different values depending on the used liquid phase. The reason for this is the significant difference in its physical properties.

The next step in the research should be a further analysis of the influence of physical properties on the drag coefficient in a wider range of physical properties of the media. Experimenting with different values of liquid viscosity, density and surface tension may contribute to better understanding of the influence of this parameters. This, in turns, may allow to determine a unified correlation for the drag coefficient for bubbles formed in the co-flowing liquid.

References

Chuang, S.C.; Goldschmidt, V.W., 1970, Bubble formation due to a submerged capillary tube in quiescent and coflowing streams, J. Basic Eng., 92, 4, 705–711.

Hadamard, J.S., 1911, Mouvement permanent lent d'une sphère liquide et visqueuse dans un liquide visqueux, Comptes rendus de l'Académie des Sciences, 152, 1735–1752.

Kulkarni, A.A.; Joshi, J.B., 2005, Bubble Formation and Bubble Rise Velocity in Gas-Liquid Systems: A Review, Ind. Eng. Chem. Res., 44, 16, 5873–5931.

Luty, P.; Prończuk, M., 2020, Determination of a bubble drag coefficient during the formation of single gas bubble in upward coflowing liquid, Processes, 8, 8, 999.

Merchuk, J.C., 2003, Airlift bioreactors: Review of recent advances, Can. J. Chem. Eng._, 81, 324–337.

Muilwijk, C.; Van den Akker, H.E.A., 2019, Experimental investigation on the bubble formation from needles with an without liquid co-flow, Chem. Eng. Sci., 202, 318–335.

Nishino, K.; Kato, H.; Torii, K., 2010, Stereo imaging for simultaneous measurement of size and velocity of particles in dispersed two-phase flow, Meas. Sci. Technol., 11, 633–645.

Sada, E.; Yasunishi, A.; Katoh, S.; Nishioka, M., 1978, Bubble formation in flowing liquid, Can. J. Chem. Eng., 56, 6, 669–672.

Terasaka, K.; Tsuge, H.; Matsue, H., 1999, Bubble Formation in Cocurrently Upward Flowing Liquid, Can. J. Chem. Eng., 77, 3, 458–464.